Interfacial Nonradiative Energy Transfer in Responsive Core−Shell Hydrogel Nanoparticles

Daoji Gan and L. Andrew Lyon*

Contribution from the School of Chemistry and Biochemistry, Georgia Institute of Technology, Atlanta, Georgia 30332-0400

Received April 9, 2001. Revised Manuscript Received July 5, 2001

Abstract: Fluorescently labeled core−shell latex particles composed mainly of the thermoresponsive polymer poly-*N*-isopropylacrylamide (p-NIPAm) have been synthesized such that an energy transfer donor (phenanthrene) and an energy transfer acceptor (anthracene) are covalently localized in the core and shell, respectively. When the thermally induced particle deswelling is interrogated by photon correlation spectroscopy (PCS), a continuous (non-first order) phase transition is observed. Conversely, when the nonradiative energy transfer (NRET) efficiency is used to probe the collapse of these same particles, the phase transition event is observed to occur over a much smaller temperature range and approaches first-order (discontinuous) behavior. Furthermore, core−shell particles with differing shell thicknesses display identical phase transition temperatures when PCS is used to monitor the transition, while NRET measurements show a clear increase in collapse temperature as the shell thickness is increased. These apparently contradictory results are discussed in terms of a radial phase coexistence that exists in the microgel particles, which arises from a similarly radial inhomogeneity in the cross-linker concentration. The prospects for the NRET technique as a molecular-scale probe of nanostructured microgels are also discussed.

Introduction

In view of the growing interest in stimuli-responsive polymers[1] for applications as diverse as drug delivery,[2] biosensing,[3] chemical separations,[4] cell culture substrates,[5,6] biomaterials,[7] and catalysis,[8] the need to fine-tune the chemical, mechanical, and structural characteristics of such materials has also increased. Particularly intriguing subclasses of responsive polymers are hydrogel latex particles, or microgels, composed of polymers such as poly-*N*-alkylacrylamides.[9] These spherical particles display a strong thermoresponsivity, where below a characteristic lower critical solution temperature (LCST) they are highly swollen in water, but upon increasing the temperature above the LCST they rapidly deswell to a collapsed polymer globule. The phase transition is rapid due simply to the reduced dimensions of the microgel, as diffusion of water from the material largely determines the rate of deswelling. In large part, these colloidal materials are of interest due to the wide range of physical properties that are modulated by the phase transition, including the hydrophobicity, particle size, porosity, refractive index, colloidal stability, scattering cross-section, electrophoretic mobility, and rheology.[9]

Our approach to the design of tunable microgels is focused on the creation of spherical core−shell architectures where the chemical identity of the shell can greatly influence the physicochemical properties of the particle as a whole.[10] The prototypical thermoresponsive polymer, poly-*N*-isopropylacrylamide (p-NIPAm),[1] is used as the building block for these particles. Previously, we have reported the creation of core−shell hydrogel particles by two-stage free radical precipitation polymerization.[10,11] In those studies, we demonstrated that the position and number of LCST values displayed by microgels could be manipulated via addition of a thin shell of dissimilar hydrogel to a gel core.[10] We have also recently demonstrated that small chemical modifications made to the shell could result in large change of the deswelling kinetics *without* perturbation of the deswelling energetics.[11] However, due to the structural complexity of the particles that result from these synthetic methodologies, further investigations are desired for the understanding of the particle deswelling. Specifically, a better knowledge of the core−shell interfacial structure and how that interface changes upon particle deswelling is of great importance in the development of multifunctional or multiresponsive microgels. In this contribution, we exploit the synthetic techniques used in the creation of core−shell particles to spatially localize nonradiative energy transfer (NRET) fluorophores within the microgel core and shell, such that thermo-induced changes in the core−shell interface are directly probed by energy transfer across that interface. Comparison of these results with (interface insensitive) PCS measurements of particle deswelling,

* To whom correspondence should be addressed: lyon@chemistry.gatech.edu.

(1) Shibayama, M.; Tanaka, T. *Volume Phase Transition and Related Phenomena of Polymer Gels*; Springer-Verlag: Berlin, 1993; Vol. 109, pp 1−62.

(2) Hoffman, A. *"Intelligent" Polymers*; Park, K., Ed.; American Chemical Society: Washington, D.C., 1997; pp 485−498.

(3) Miyata, T.; Asami, N.; Uragami, T. *Macromolecules* **1999**, *32*, 2082−2084.

(4) Tanaka, T.; Wang, C.; Pande, V.; Grosberg, A. Y.; English, A.; Masamune, S.; Gold, H.; Levy, R.; King, K. *Faraday Discuss.* **1995**, *101*, 201−206.

(5) Kwon, O. H.; Kikuchi, A.; Yamato, M.; Sakurai, Y.; Okano, T. *J. Biomed. Mater. Res.* **2000**, *50*, 82−89.

(6) Yamato, M.; Kwon, O. H.; Hirose, M.; Kikuchi, A.; Okano, T. *J. Biomed. Mater. Res.* **2000**, *55*, 137−140.

(7) Burczak, K.; Gamian, E.; Kochman, A. *Biomaterials* **1996**, *17*, 2351−2356.

(8) Bergbreiter, D. E.; Case, B. L.; Liu, Y.-S.; Caraway, J. W. *Macromolecules* **1998**, *31*, 6053−6062.

(9) Pelton, R. *Adv. Colloid. Interface Sci.* **2000**, *85*, 1−33.

(10) Jones, C. D.; Lyon, L. A. *Macromolecules* **2000**, *33*, 8301−8306.

(11) Gan, D.; Lyon, L. A. *J. Am. Chem. Soc.* **2001**, *123*, 7511−7517.

10.1021/ja015974l CCC: $20.00
Published on Web 08/02/2001

along with previous studies of hydrogel morphology, allows for a greater understanding of microgel collapse events.

Experimental Section

Materials. All the reagents were purchased from Aldrich unless otherwise stated. *N*,*N*-dimethylformamide (DMF) was distilled under reduced pressure. Both triethylamine and pyridine were dried and then distilled from sodium under nitrogen. Tetrahydrofuran (THF) was obtained from J. T. Baker and distilled from sodium/benzophenone. *N*-Isopropylacrylamide (NIPAm) (J. T. Baker) was recrystallized from hexane before use. Anthrone, phenanthracene-9-carboxaldehyde, sodium borohydride, methacryloyl chloride, *N*,*N*′-methylenebis(acrylamide) (BIS), sodium dodecyl sulfate (SDS), and ammonium persulfate (APS) were used as received. (9-Phenanthryl)methyl methacrylate (PheMMA) was synthesized via the reaction of phenanthrylmethanol (reduction product of phenanthracene-9-carboxaldehyde by sodium borohydride) with methacryloyl chloride using THF and triethylamine as a solvent and a catalyst, respectively.[12] (9-Anthryl)methacrylate (AnMA) was prepared by reacting anthrone with methacryloyl chloride in THF in the presence of dried pyridine.[13] Water used in all syntheses and measurements was distilled and then purified using a Barnstead E-Pure system operating at a resistance of 18 MΩ. A 0.2 μm filter was incorporated into this system to remove particulate matter.

Polymerization. The particles were prepared via free-radical, precipitation polymerization, with 5 mol-% (based on NIPAm used) BIS as a cross-linker and 1 mol-% APS as an initiator. A detailed procedure was described elsewhere.[10,11,14] Briefly, 1.13 g (10 mmol, 1 equiv) of NIPAm (monomer), BIS (cross-linker), and SDS (surfactant) were introduced into 150 mL of degassed water along with the appropriate amount of fluorescent comonomer (PheMMA or AnMA) predissolved in DMF at a concentration of 5 mg/mL. The reaction mixture was maintained at 70 °C with nitrogen bubbling for 2 h. The polymerization was then carried out at 70 °C for 6 h under a stream of nitrogen. Under these synthesis conditions, the monomers are all highly soluble. However, following the addition of APS (initiator), the solution becomes turbid as the growing oligomers reach their critical aggregation length, upon which phase separation into collapsed chains occurs. These collapsed globules act as nuclei for particle formation as polymerization continues. This method of precipitation polymerization produces submicron-sized, spherical network hydrogels (microgels).[9,15−17]

Core−shell particles were prepared by a two-stage (seed and feed) polymerization, in which particles prepared by the method described above were used as seed particles during the reaction of a second feed of monomer, comonomer, cross-linker, surfactant and initiator. Under the conditions of polymerization (aqueous solution at 70 °C) these added monomers are highly soluble in the continuous phase and do not partition strongly into the collapsed polymer seed particles. However, when the monomers polymerize into a growing oligoradical, they can be captured by the seed particles upon reaching the critical length at which phase separation of the polymer occurs. In this fashion, one can create microgels that have layered or core−shell structures, as previously demonstrated by TEM studies.[10] While some core−shell interpenetration almost certainly occurs upon reswelling (cooling), previous studies, and the results presented below suggest that such interpenetration is not a dominant effect.[10] The chemical compositions and hydrodynamic radii of particles prepared in this fashion are listed in Table 1.

To minimize effects due to variability in core size on the phase-transition measurements, core−shell particles (CS1−CS3) were constructed using the same batch of core particles, which is reflected by the identical core sizes within that series. The shell thickness was controlled by adjusting the amounts of monomer in the feed, and by varying the concentration of SDS (from 0.001 to 0.02 equiv based on NIPAm) during the second stage of polymerization. In general, higher concentrations of SDS result in thinner shells, as predicted by nucleation theory.[16,18] All particles were purified via dialysis (Spectra/Por 7 dialysis membrane, MWCO 10000, VWR) first against water/DMF (volume ratio: 80/20) for 7 days and then against pure water for an additional 14 days, with daily replacement of the dialyzed liquid.

Table 1. Chemical Compositions and Radii of Fluorescently Labeled Hydrogel Particles[a]

code	core (molar ratio): NIPAm/PheMMA/AnMA	R_{core} (nm)[b]	shell (molar ratio): NIPAm/PheMMA/AnMA	$R_{core-shell}$ (nm)[b]
C	100/0.5/0	160	-	-
CS	100/0.5/0	160	100/0/0.5	201
C_{DA}	100/0.25/0.25	165	-	-
CS1	100/0.5/0	169	100/0/0.5	185
CS2	100/0.5/0	169	100/0/0.5	230
CS3	100/0.5/0	169	100/0/0.5	400

[a] All particles were synthesized using 5 mol-% BIS (based on NIPAm) as a cross-linker; Sample C is the core particle used to construct Sample CS, and CS1−CS3 were prepared using the same batch of core particles, which was reflected by the identical sizes of the cores. [b]Particle radii were measured using PCS in water at 25 °C.

Photon Correlation Spectroscopy. Particle sizes in aqueous solution were determined by PCS (Protein Solutions, Inc.), as described previously.[10,11,14] The water-dispersed particles were maintained at each temperature for 10 min before measurements were taken. Longer equilibration times did not result in differences in the observed hydrodynamic radii, polydispersities, or scattering intensities. In the data presented below, each point at a given temperature represents the average value of 10−20 measurements, with a 10−20 s integration time for each measurement (signal-to-noise levels, which are determined by the integration time, were optimized for each sample while attempting to minimize the total analysis time). Error bars were calculated from the standard deviation about the mean of five such measurements. Hydrodynamic radii were calculated from the measured diffusion coefficients using the Stokes−Einstein equation.[19] All correlogram analyses were performed with manufacturer-supplied software (Dynamics v.5.25.44, Protein Solutions, Inc.). In some cases, size changes were converted to a volume deswelling ratio (V/V^*), which is calculated by the relation $V/V^* = (r/r^*)^3$, where r and r^* are the averaged particle radius at the measured temperature and at 25 °C, respectively.

Fluorometry. Fluorescence spectra were recorded on a steady-state fluorescence spectrophotometer (Photon Technology International), equipped with a Model 814 PMT photon-counting detector. The temperature control was achieved using a PE 60 Temperature Controller & Peltier Stage (Linkam Scientific Instruments Ltd., Surrey, UK). The solution temperature was measured with a platinum resistor as a temperature sensor immersed in the sample solution, and the temperature accuracy was in the range of ± 0.1 °C as specified by the manufacturer. Prior to the measurements, the sample solution was stirred in a quartz cell and allowed to thermally equilibrate for 10 min at each temperature. Longer equilibration times did not result in differences in the observed spectral intensity or shape. The slits were set to achieve a spectral bandwidth of 2.5 nm, and the spectra were measured with a step size of 1 nm and a 1 s integration time. The monomer spectra (PheMMA and AnMA) were recorded at a concentration of 1.0×10^{-7} M in water, which was prepared under nitrogen atmosphere by addition of small amounts of the monomer/THF solution into the water, followed by evaporation of THF. The excitation wavelengths were 298 and 370 nm for PheMMA and AnMA, respectively. Energy transfer measurements of microgel solutions were measured at a very low concentration ($\sim 1.0 \times 10^{-5}$ g/L) in order to reduce the influence of scattering from

(12) Ng, D.; Guillet, J. E. *Macromolecules* **1982**, *15*, 728−732.
(13) Zhao, C. L.; Wang, Y. C.; Hruska, Z.; Winnik, M. A. *Macromolecules* **1990**, *23*, 4082−4087.
(14) Debord, J. D.; Lyon, L. A. *J. Phys. Chem. B* **2000**, *104*, 6327−6331.
(15) Saunders, B. R.; Vincent, B. *Adv. Colloid Interface Sci.* **1999**, *80*, 1−25.
(16) Wu, X.; Pelton, R. H.; Hamielec, A. E.; Woods, D. R.; McPhee, W. *Colloid Polym. Sci.* **1994**, *272*, 467−477.
(17) Crowther, H. M.; Saunders: B. R.; Mears, S. J.; Cosgrove, T.; Vincent, B.; King, S. M.; Yu, G. E. *Colloid Surf. A-Physicochem. Eng. Asp.* **1999**, *152*, 327−333.
(18) McPhee, W.; Tam, K. C.; Pelton, R. *J. Colloid Interface Sci.* **1993**, *156*, 24−30.
(19) Pecora, R. *Dynamic Light Scattering*; Plenum Press: New York, 1985.

the particles. The excitation wavelength was chosen to be 298 nm for interrogation of all microgel samples. Particle phase transitions are reported in terms of the ratio of the emission intensity at 370 nm (I_D) to that at 413 nm (I_A); these wavelengths are largely associated with emission from the energy donor (PheMMA) and the energy acceptor (AnMA), respectively.

Results

In our previous studies, microgel volume phase transitions were typically interrogated by techniques such as PCS or differential scanning calorimetry (DSC).[10,11,14] These techniques are largely insensitive to any nanoscale heterogeneity present in the particles. For example, it has been theorized that the breadth of microgel volume phase transitions are due to a radial cross-linker density gradient, where a higher cross-linker concentration persists at the particle center, and a lower density exists at the periphery. Such a gradient has been proposed upon detailed analysis of the polymerization mechanism[16] and more recently has been inferred from NMR, PCS and turbidity studies.[20−22] Since increasing the cross-linker density results in an increase in the volume phase transition temperature, it has been proposed that the particle periphery (lower cross-link density) undergoes a phase transition at lower temperature, while the particle interior collapses at higher temperatures, thereby resulting in an "outside-in" collapse mechanism. It is important to note that this argument is not based on dynamic events such as the diffusion rate of water from the gel, but rather follows from a rigorous thermodynamic description of microgel deswelling.[23,24] Since such network heterogeneity has been theorized previously for simple microgels,[16,20−24] and even greater structural heterogeneity is present in core−shell particles, we employed NRET measurements to probe hydrogel swelling at nanometer length-scales in order to gain a better understanding of the deswelling thermodynamics. Fluorescence techniques, especially energy transfer studies, have been widely used in static and dynamic studies of both natural and synthetic polymers.[25−31] NRET is a process by which energy is transferred between a photoexcited chromophore and a ground-state chromophore via a dipole−induced dipole interaction. As such, there are three primary conditions for the energy transfer to occur: (1) the donor and the acceptor should be in close proximity, (2) the relative donor−acceptor orientation should be such that their transition dipole moments are not orthogonal, and (3) there should be spectral overlap between the donor emission and the acceptor absorption.[32] For the purposes of this study, a polymerizable donor (PheMMA) and acceptor (AnMA) were used as comonomers in the synthesis of p-NIPAm microgels. The structures of these two monomers are shown in Chart 1.

Chart 1. Chemical Structures of the Fluorescence Donor (PheMMA) and Acceptor (AnMA) Monomers

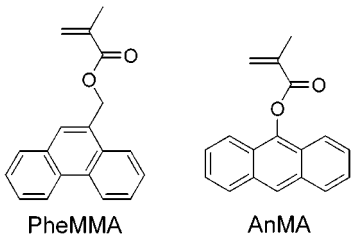

To ascertain the behaviors of these fluorophores prior to polymerization, the photophysical properties of the donor and the acceptor in water were investigated. Shown in Figure 1 are the overlaid emission spectra of PheMMA and AnMA at a concentration of 1×10^{-7} M in water. When excited at 298 nm, the spectrum of PheMMA shows characteristic fine structure, with a maximum peak at 370 nm. Excitation of AnMA at 370 nm yields an emission spectrum with three distinguishable peaks, the largest being centered at 413 nm. Because of the strong spectral overlap between the donor emission and the acceptor absorption spectra, PheMMA and AnMA should behave as a good fluorescence donor/acceptor pair, a property that has been demonstrated previously.[13,33] Given the mechanism of NRET, it has been shown that the efficiency of energy transfer is governed by the relation:

$$E = R^6/(R^6 + r^6) \quad (1)$$

where R is the characteristic Förster distance between the donor and the acceptor at which the efficiency of transfer decays to 0.5, and r is the actual distance between the donor and the acceptor.[33] Previous investigations by other groups have measured the Förster distance for the phenanthrene−anthracene couple to be approximately 2.3 nm.[33] Thus we can reasonably expect the energy transfer from the donor to the acceptor to occur in the range of 0−5 nm.

Core−shell microgels composed of p-NIPAm-based copolymers were synthesized via two-stage, free-radical precipitation polymerization initiated with APS at 70 °C in water. Since this temperature is much higher than the LCST of p-NIPAm, the polymer precipitates to form spherical particles. These particles can then be used as seed particles in a second polymerization reaction. We have shown previously that under our reaction conditions, the deposition of polymer onto preexisting nuclei is greatly preferred over the formation of new nuclei.[10] Thus, this procedure affords preparations of core−shell particles with nearly identical polydispersities to the core particles from which they were synthesized. Fluorescently labeled microgels were prepared by copolymerization of ∼0.5 mol-% PheMMA or AnMA (based on the amount of NIPAm) into the particles. For the purposes of this study, six different microgel samples were prepared; the compositions and sizes of these particles are listed in Table 1.

The thermoresponsivities of p-NIPAm-*co*-PheMMA core, and p-NIPAm-*co*-PheMMA/p-NIPAm-*co*-AnMA core/shell particles are shown in Figure 2a. It is noteworthy that the addition of the shell does not induce an LCST shift, or a change in the curve breadth (∼5 °C), and only produces the expected increase in size for both the swollen and collapsed states. Furthermore, the LCST values obtained here are identical to those obtained

(20) Guillermo, A.; Addad, J. P. C.; Bazile, J. P.; Duracher, D.; Elaissari, A.; Pichot, C. *J. Polym. Sci. Pt. B−Polym. Phys.* **2000**, *38*, 889−898.
(21) Duracher, D.; Elaissari, A.; Pichot, C. *Colloid Polym. Sci.* **1999**, *277*, 905−913.
(22) Duracher, D.; Elaissari, A.; Pichot, C. *Macromol. Symp.* **2000**, *150*, 305−311.
(23) Wu, C.; Zhou, S. *Macromolecules* **1997**, *30*, 574−576.
(24) Wu, C. *Polymer* **1998**, *39*, 4609−4619.
(25) Morawetz, H. *J. Lumin.* **1989**, *43*, 59−71.
(26) Morawetz, H. *Science* **1988**, *240*, 172−176.
(27) Smith, G. L.; McCormick, C. L. *Macromolecules* **2001**, *34*, 918−924.
(28) Yang, J.; Winnik, M. A.; Ylitalo, D.; DeVoe, R. J. *Macromolecules* **1996**, *29*, 7047−7054.
(29) Principi, T.; Goh, C. C. E.; Liu, R. C. W.; Winnik, F. M. *Macromolecules* **2000**, *33*, 2958−2966.
(30) Winnik, F. M.; Regismond, S. T. A. *Colloid Surf. A-Physicochem. Eng. Asp.* **1996**, *118*, 1−39.
(31) Charreyre, M. T.; Tcherkasskaya, O.; Winnik, M. A.; Hiver, A.; Delair, T.; Cros, P.; Pichot, C.; Mandrand, B. *Langmuir* **1997**, *13*, 3103−3110.
(32) Lakowicz, J. R. *Principles of Fluorescence Spectroscopy*; 2nd ed.; Kluwer Academic: New York, 1999.
(33) Perez, E.; Lang, J. *J. Phys. Chem. B* **1999**, *103*, 2072−2084.

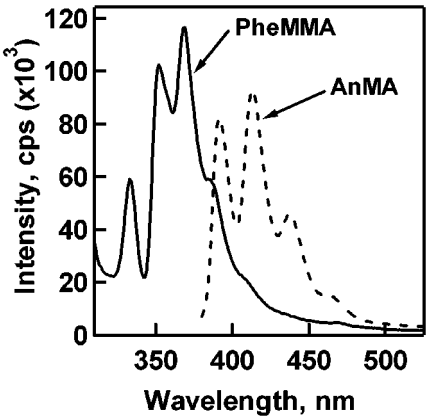

Figure 1. Fluorescence spectra of the donor, PheMMA (λ_{ex} = 298 nm) and the acceptor, AnMA (λ_{ex} = 370 nm) at a concentration of 1 × 10^{-7} M in water.

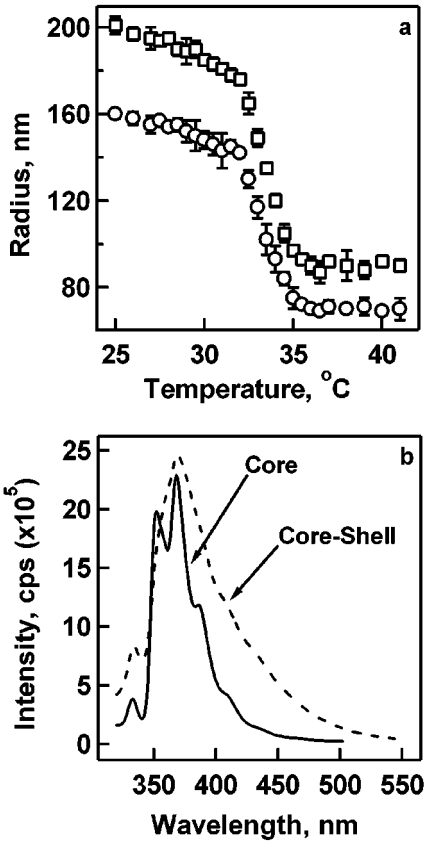

Figure 2. (a) Core (circles) and core−shell (squares) particle radii as a function of temperature, as measured by PCS in water. Error bars represent the standard deviation of five measurements. Where error bars are absent, the symbol size is greater than the standard deviation. (b) Fluorescence spectra of the particles at 25 °C in water with excitation at 298 nm. The chemical compositions of samples C and CS are shown in Table 1.

for microgels that are not fluorescently labeled; the hydrophobic fluorophores do not change the hydrogel deswelling thermodynamics at the concentrations used here. When the fluorescence of the PheMMA-labeled core is measured at 25 °C (298 nm excitation, Figure 2b) the same characteristic fine-structure is observed as was seen for PheMMA in water (Figure 1). In contrast, interrogation of the fluorescence at the same excitation wavelength and temperature following the addition of the AnMA-labeled shell shows a disappearance of the fine structure in the PheMMA spectrum, as well as a small increase in the intensity at wavelengths longer than 370 nm (Figure 2b).

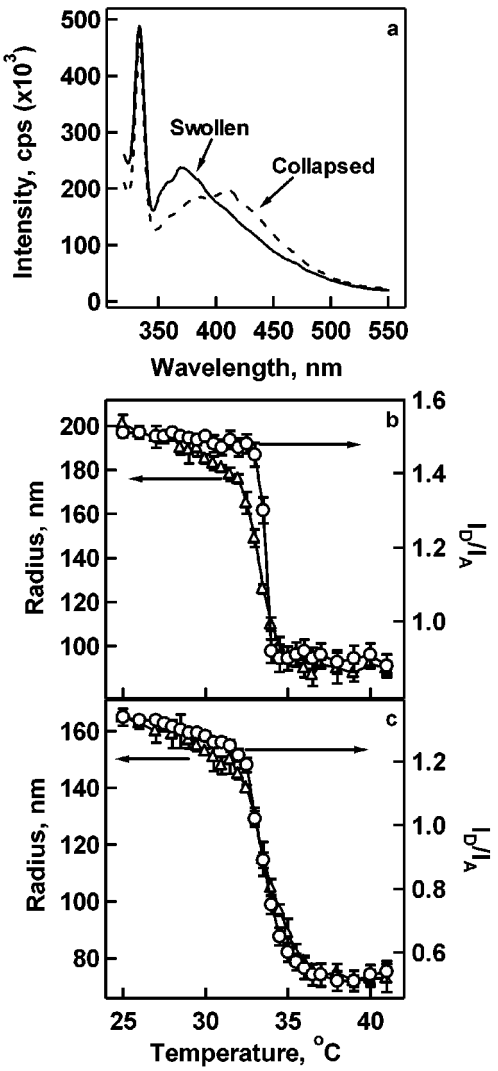

Figure 3. (a) Fluorescence spectra (λ_{ex} = 298 nm) of Sample CS in water at 25 °C (swollen) and 40 °C (collapsed). Corresponding plots of the donor/acceptor intensity ratio (circles) and the particle radii (triangles) as a function of temperature are shown in (b) for Sample CS and (c) for Sample C_{DA}, p-NIPAm-*co*-PheMMA-*co*-AnMA. Error bars represent the standard deviation of five measurements. Where error bars are absent, the symbol size is greater than the standard deviation.

When the microgels are excited at 298 nm and the resultant fluorescence is monitored as a function of temperature, significant changes in the shape of the spectrum are observed. An intensity decrease below ∼380 nm is accompanied by an increase in fluorescence above that wavelength (Figure 3a). Plotting the ratio of the intensities at 370 nm (PheMMA emission) and 413 nm (AnMA emission) as a function of temperature yields the phase transition curve shown overlaid with the PCS determined curve in Figure 3b. It is evident from these data that the deswelling observed for p-NIPAm-*co*-PheMMA(core)/p-NIPAm-*co*-AnMA(shell) microgels is strongly dependent on the measurement technique; observation of phenanthrene−anthracene energy transfer efficiency yields a much sharper transition than that measured by PCS. Furthermore, the LCST (defined as the collapse midpoint) measured by these techniques also fails to be self-consistent, as the NRET-obtained value is slightly higher than the PCS value. In contrast to these results, however, a particle containing a random (non-core−shell) distribution of donor and acceptor displays the same transition temperature and breadth regardless of inter-

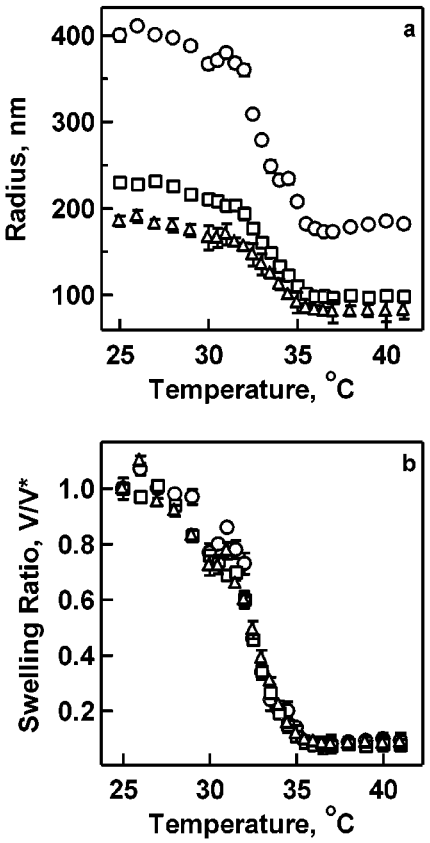

Figure 4. Temperature-dependent particle radii (a) and deswelling ratios (b) of p-NIPAm-*co*-PheMMA(core)/p-NIPAm-*co*-AnMA(shell) particles with varying shell thicknesses [CS1 (triangles), CS2 (squares), and CS3 (circles)]. Details of the particle compositions are listed in Table 1. Error bars represent the standard deviation of five measurements. Where error bars are absent, the symbol size is greater than the standard deviation.

rogation method (sample C_{DA}, p-NIPAm-*co*-PheMMA-*co*-AnMA (core), Figure 3c).

Since the data presented above seem to suggest that the core−shell morphology is responsible for the measurement-dependent observations, a series of donor(core)−acceptor(shell) particles were synthesized, where different shell thicknesses were added to particles from the same batch of core microgels (CS1−CS3). Measurement of the particle size as a function of temperature via PCS yields the curves shown in Figure 4a. As with the core−shell particles described above, the PCS data show size increases for both the swollen and collapsed particles, indicative of the addition of a hydrogel shell to the core particle. When these data are normalized with respect to the relative volume change (Figure 4b), the three curves show a striking similarity, as the LCST value (∼32 °C), the curve breadth (∼5 °C), and the magnitude of the transition is identical for the three particle sizes.

Figure 5 shows a comparison of the phase transitions for these three particles as measured by PCS and fluorescence. Again, when the phase transition is monitored via NRET, an extremely sharp transition is observed despite the significant breadth of the PCS curve. Furthermore, the relative position of the two curves differs among the three particle sizes. For the thinnest shell (16 nm added radius), the NRET-obtained phase transition occurs at a temperature lower than the LCST, while the two thicker shells (61 and 231 nm added) display LCST values that are equal to and higher than the LCST, respectively. This shift in NRET-measured LCST is clearly shown in Figure 6.

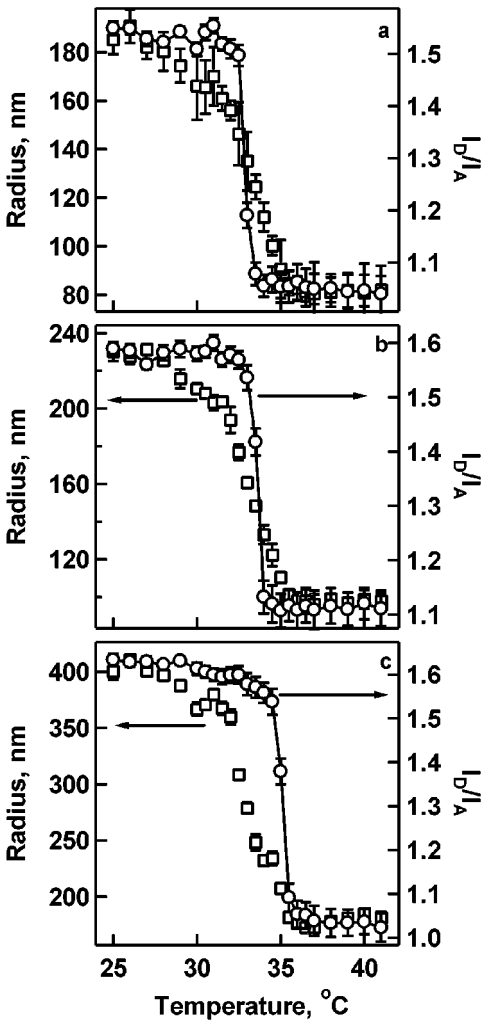

Figure 5. Plots of particle radii (squares) and fluorescence intensity ratios (circles) as a function of temperature for (a) CS1, (b) CS2, and (c) CS3. The fluorescence-measured LCST increases as the shell thickness increases while the PCS curves remain constant. Error bars represent the standard deviation of five measurements. Where error bars are absent, the symbol size is greater than the standard deviation.

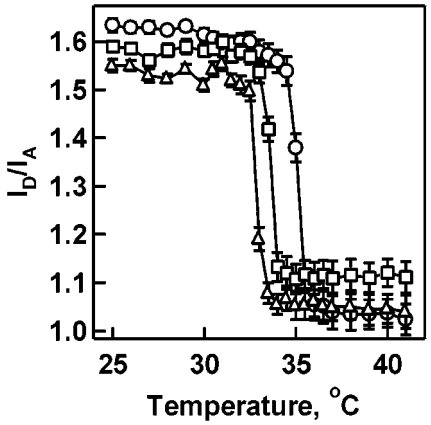

Figure 6. Fluorescence intensity ratios as a function of temperature for CS1 (triangles), CS2 (squares), and CS3 (circles). Error bars represent the standard deviation of five measurements. Where error bars are absent, the symbol size is greater than the standard deviation.

Discussion

Nonradiative energy transfer has been used in a wide variety of polymeric systems in order to gain dynamic and morphologi-

Scheme 1. Proposed Mechanism of Core−Shell Microgel Deswelling

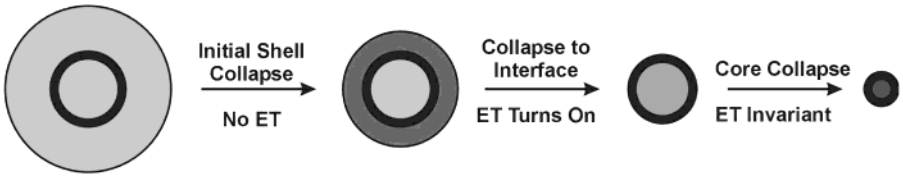

cal information at the nanometer scale.[13,31,34,35] In the experiments described above, a simple donor−acceptor pair was chosen for the purpose of gaining a fundamental understanding of the thermodynamic mechanism of microgel deswelling and to interrogate the core−shell microgel interface. It is interesting to note that the spectrum of the core alone looks very similar to that of the unpolymerized PheMMA monomer in aqueous solution (Figure 2b). However, upon addition of a shell containing the AnMA acceptor, the spectrum changes significantly. Inspection of the monomeric spectra of the donor and acceptor (Figure 1) suggests that these spectral changes are due to a weak anthracene fluorescence convoluted with the relatively strong phenanthrene emission. Since the excitation wavelength is resonant only with phenanthrene absorption, the anthracene emission must arise from a small amount of energy transfer from phenanthrene to anthracene. As the length-scale over which energy transfer occurs efficiently is only a few nanometers, we attribute this low level of energy transfer to a relatively small percentage of donor and acceptor molecules localized close to one another at the core−shell interface. This result is significant in that it suggests that the monomer from the shell synthesis does not partition strongly into the seed particles. If significant partitioning and interpenetration did occur, one would expect to see greatly enhanced energy transfer due to the greater proximity of the donor and acceptor fluorophores. Indeed, the sample with homogeneously distributed donor and acceptor in a core particle alone (C_{DA}) required the use of 2-fold lower fluorophore concentrations in order to reduce the energy transfer efficiency to a level similar to that of the core−shell particles.

The situation becomes a bit more complex when the energy transfer efficiency is measured as a function of temperature. Unlike the bulk swelling behavior as measured by PCS, which displays a continuous deswelling event, NRET measurements suggest a discontinuous transition. As described above, it is well-known that the p-NIPAm microgels display a broader phase-transition curve in comparison to either semidilute solutions of linear polymer or homogeneous monolithic gels.[23,24] A powerful argument for the origin of this effect points to heterogeneity in the length of subchains in the microgel network as a possible cause.[23] It has been proposed that the subnetworks having longer chains undergo their phase transition at a lower temperature than those with shorter chain lengths. Accordingly, the measured phase transition curve is really a convolution of many transitions, with each subnetwork having its own characteristic transition temperature.[23,24] In light of this explanation, we can see that the extreme sharpness of the NRET-monitored transition reflects a localization of the donor and acceptor molecules within a subnetwork possessing a narrower chain-length distribution. The fact that the observed LCST differs from that measured by PCS simply indicates that the subnetwork being probed does not deswell at the average deswelling temperature. Conversely, when the phenanthrene and anthracene groups are distributed randomly throughout the gel (Figure 3c), the NRET process samples a distribution of subchain lengths that is representative of the particle as a whole.

Despite this explanation, it is still not clear why localization of the fluorophores in a thin spherical shell (the interface) necessarily localizes them in a *single narrow subnetwork domain.* An explanation for this can be constructed, however, if we examine the most likely spatial distribution of chain lengths. In large part, an argument can be made by simply invoking the relative reaction rates of NIPAm and BIS. Since BIS contains two acrylate groups available for polymerization, it should react at approximately twice the rate of NIPAm.[16,18] Furthermore, particle growth in precipitation polymerization is known to occur via a radial growth mechanism. Therefore, the combination of fast BIS consumption with "inside-out" growth should lead to a material with greater cross-link density near the center of the particle. This morphology has been proposed previously, and evidence for it has been obtained by NMR relaxation experiments.[20] Combining these observations, it's reasonable to assume that microgel collapse starts at the particle periphery and gradually deswells toward the more densely cross-linked center. As a result, the core−shell interface will always lie in a region of the particle that has the same narrow chain length distribution. A graphical depiction of this deswelling process is shown in Scheme 1. In the scheme, the particle is depicted as first deswelling in the peripheral region; the average number of donor/acceptor pairs within the Förster radius does not increase in this process. The next stage is collapse to the interface. In this step, the loss of solvent in the region of closest donor−acceptor contact results in more efficient NRET. Finally, the particle core deswells to the completely collapsed state. Since all of the donor−acceptor pairs that are within one Förster radius of each other have already reached that limiting configuration, no increase in energy transfer is observed. It is important to remember that the Förster radius is less than 1% of the total particle radius. Therefore, only a very small volume of the hydrogel, that which is localized at the core−shell interface, will ever participate in NRET.

This mechanism aids in the interpretation of the shell thickness dependence (Figures 6 and 7). As described above, as there is an increase in the shell thickness, the phase transition determined by fluorescence technique shifts to a higher temperature, while the PCS data shows shell thickness invariant deswelling behavior. Furthermore, the NRET phase transition temperature always lies within temperatures defined by the broad deswelling transition measured by PCS. Given that these core−shell particles were built upon the same size core particles, and determination of the LCST using PCS gave identical phase transition curves, the difference in the phase transitions observed by NRET should be related to variation in the thickness of the acceptor-containing shell. Since deswelling of the particles proceeds from the microgel periphery to the center, and energy transfer occurs only in the thin interfacial layer, the particles having a thick shell must deswell a greater percentage of their volume before reaching the interface. Accordingly, the particles with the thickest shells display interfacial collapse much later in the overall phase transition than those with the thinner shells.

(34) Rharbi, Y.; Yekta, A.; Winnik, M. A.; DeVoe, R. J.; Barrera, D. *Macromolecules* **1999**, *32*, 3241−3248.
(35) Polozova, A.; Winnik, F. M. *Biochim. Biophys. Acta* **1997**, *1326*, 213−224.

However, this explanation does not satisfactorily explain the invariance in LCST with shell thickness. If the core particle possesses a specific distribution of subchain lengths that produce a characteristic LCST curve, why upon shell addition does the core suddenly choose to deswell at higher temperatures (as reflected by the increase in the NRET-measured LCST)? This can be understood if we invoke the synthetic method employed in the core−shell synthesis. Two-stage precipitation polymerization requires that the core particle be *deswollen* during addition of the shell in order to achieve efficient nucleation. However, if the first layers of shell polymer have a very high cross-linker content, which is a reasonable assumption given the relative reaction rate argument stated above, the shell will physically restrict the core to a density far higher than it previously possessed. In other words, despite the fact that the original core had a very long average chain length near the particle periphery, those chains are strongly compressed during the second polymerization stage and will therefore show very similar deswelling thermodynamics to that of a highly cross-linked network. As a result, we can reasonably expect that all microgels synthesized in this way with identical cross-linker concentrations will yield nearly identical radial subchain distributions, with that distribution being largely determined by the nature of the shell.

Conclusions

In this study, we have demonstrated the utility of NRET measurements in the elucidation of the microgel deswelling mechanism. While PCS is a useful method for understanding microgel solvation on the particle length-scale, NRET allows for interrogation of a specific region of the material, thereby providing a means for the study of nanoscale heterogeneity in such materials. Specifically, we have shown that microgels deswell in a radially heterogeneous fashion, beginning with the particle periphery and proceeding to the core. Furthermore, addition of a hydrogel shell to a microgel core results in compression of the core and a corresponding modulation of the core deswelling thermodynamics. This is reflected by a shell thickness independent LCST as measured by PCS, but a strong thickness dependence when NRET is used to probe the interfacial collapse. These results illustrate the tremendous complexity that can be achieved in relatively simple nanostructured soft materials and point toward the factors that control such complexity. We are currently investigating the deswelling mechanisms of more complex architectures, such as those possessing multiple phase transitions[10] in response to a single stimulus. It is expected that such studies will significantly improve our understanding of responsive hydrogel nanostructures.

Acknowledgment. L.A.L. gratefully acknowledges financial support from Research Corporation in the form of a Research Innovation Award, from the National Science Foundation for a CAREER Award, and from the Arnold and Mabel Beckman Foundation for a Young Investigator Award.

JA015974L